Nucleic Acids Research, 2026, **54**, gkaf1539
https://doi.org/10.1093/nar/gkaf1539
Nucleic Acid Therapeutics

Staufen dsRNA-binding domain as modules to design bifunctional antibodies for siRNA delivery

Yahui Liu†, Yan Zheng†, Ruolin Xu, Yanan Quan, Wanyi Tai*

Department of Pharmaceutical Engineering, School of Pharmaceutical Sciences, Wuhan University, Wuhan, Hubei 430071, China

*To whom correspondence should be addressed. Email: wanyi-tai@whu.edu.cn
†The first two authors should be regarded as Joint First Authors.

Abstract

Antibody–small interfering RNA (siRNA) conjugates present an opportunity to expand the siRNA therapy to extrahepatic tissues. However, their investigation is now only confined to a limited number of targets, partially owing to some flaws in structures. Here, we described a modular design of bifunctional antibody that tethers siRNA without conjugation, yielding a diligent one-to-one antibody–siRNA pairing structure feasible for target expansion, charge masking, and further functionalization. Focusing on a noncationic siRNA-recruiting module, Staufen1 dsRBD34, we demonstrated that bifunctional antibodies recruit siRNA independent of base modification and enable target gene silencing on multiple cell types at a stoichiometry (1/1). Notably, by functionalizing siRNA terminus with small-molecule enhancers, the silencing potency of this pairing system can be augmented by seven times (IC_{50} from 200 to 28 nM) through the endosome-to-cytosol import. Affinity maturation by arginine scanning yields the 32 times higher affinity of dsRBD34 to siRNA, but the augment led to neither stronger silencing nor higher stability in mouse plasma as compared to p19 protein. The competition from sulfated GAGs in circulations can alter the pharmacokinetics of pairs and prevent a practical assessment of their potential *in vivo*. Altogether, bifunctional antibodies here possess notable properties, but ultrahigh-affinity dsRNA-binding domain is necessary to realize applications.

Graphical abstract

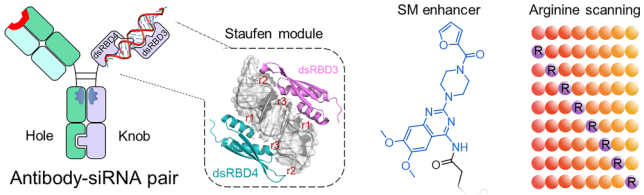

Introduction

Antibodies and small interfering RNAs (siRNAs) are two classes of biologics that have high therapeutic values in the clinic owing to their precise targeting ability. Antibody–siRNA conjugates (ARCs), which combine two biologics through covalent linkages, are now emerging as a novel modality and show promising potential to knock down disease genes beyond the liver [1]. Avidity Biosciences company develops its ARC pipeline Del-desiran (AOC1001) to treat Myotonic Dystrophy Type 1, which has entered the Phase III clinical trial (NCT06411288) in 2024. Several other ARC pipelines are also stepping into the preclinical or early clinical phases [2]. Despite the remarkable advancement in recent years, the development of ARCs remains conceptually complex and challenging because of the following reasons: (i) The current structures of ARCs lack the endosomal disrupting component, thus confining their targets to only a few antigens such as TfR1 (transferrin receptor 1), CD22, etc., otherwise noneffective in messenger RNA (mRNA) silencing [3–5]. (ii) SiRNAs are more difficult to conjugate with antibodies than chemical toxins because of the payload large size and polyanionic nature. The reported ARCs mostly have a drug-to-antibody ratio (DAR) of only ∼1, which marks a big drop from antibody–drug conjugates (ADCs) that typically have DAR values ∼4 (even 8 or more) [6, 7]. (iii) Appending of siRNAs on antibodies alters the surface charge distribution and induces a rapid clearance of ARCs from systemic circulation. (iv) The linker chemistry is restricted. SiRNA is chemically sensitive and intolerant to many organic reactions, making the linker-payload synthesis challenging. ARCs generally utilize very simple linkers such as noncleavable SMCC or disulfide SPDB, whose response to microenvironments is poorer than the new-generation ValCit-PAB or GGFG tetrapeptidyl-aminomethoxy linkers [8]. Taking all of these limitations into account, new antibody–siRNA systems might be explored to expand the applicability of siRNA for extrahepatic delivery.

Received: July 18, 2025. **Accepted:** December 16, 2025

An attractive alternative is the delivery of siRNAs by antibodies through noncovalent conjugation. This approach omits the conjugation process, which not only simplifies the synthesis steps but also endows with benefits like charge masking and endosomal disruption advantages. Due to these appealing benefits, the noncovalent antibody–siRNA complex has been investigated very early by scientists, and is even more popular than the covalent ARC strategy at the beginning. Song *et al*. reported an antibody–protamine fusion protein to deliver siRNA by coupling antibody and siRNA via charge interactions between protamine and siRNA [9–12]. Similarly, Shankar group and Scott group independently replaced the protamine with a less immunogenic $(D\text{-arginine})_9$ peptide and delivered siRNA to relevant cell types [13, 14]. As were reported, all these systems rely on cationic components to condense siRNA and achieve the noncovalent conjugation. Despite the high siRNA loading (DAR $\geq$ 5) and endosome-disrupting activity [14, 15], the generation of antibody–siRNA complex by this method relies on nonspecific electrostatic interaction and often results in heterogeneous aggregates or nanoparticlization [16, 17], which affects the selectivity, stability, clearance, toxicity, and efficacy *in vivo*. Overall, this approach represents a proof-of-concept test on the noncovalent conjugation, but significant improvements are required to meet the rigorous demands of clinical trials and manufacturing practices (GMP compliance).

The learning from the decades-long development of ADCs tells us that a diligent conjugate design, including defined structure, precise DAR value, and stable conjugation, is of high importance for developing drug candidates of clinical success [18]. As for the noncovalent antibody–siRNA approach, it requires at least the antibody to recognize and bear siRNAs independently of charges. Toward establishing a diligent noncovalent conjugate, we set out to assess the possibility of dsRNA-binding domains (dsRBDs) as antibody modules for siRNA packing and delivery. DsRBDs are a group of small protein domains found in at least 30 dsRNA-binding proteins (dsRBPs) of human cells and work in synergy with dsRNAs (including siRNAs) for biological manipulation [19]. They typically contain 65–70 amino acids (aa) and adopt an $\alpha\beta\beta\beta\alpha$ fold that recognizes the grooves of A-form dsRNAs in a shape-dependent rather than sequence-specific manner [20]. This feature is well suited to siRNAs of any target, just like the cationic condensation of any siRNA sequences by spermine and $(D\text{-arginine})_9$ peptides, but distinct from their patterns of electrostatic complexation. DsRBDs have been reported previously for siRNA delivery, but these prior designs were all supplemented with cell-penetrating peptides or protein transduction domains for a proof-of-concept demo, which are cationic and lack clinical relevance [21–23]. In this work, we selected Staufen1 (Stau1) dsRBD34 from seven human dsRBPs as the siRNA recruiter based on its superior affinity, selectivity, stability, and releasability. The Stau1 dsRBD34 is modularly constructed into bifunctional antibodies and paired with siRNAs for target-specific delivery. We demonstrated that it can silence genes in multiple types of tumor cells by free uptake (without cationic assistance), especially effectively when siRNA was functionalized by small-molecule (SM) enhancers. The knockdown effect of antibody–siRNA pairs is highly dependent on the stoichiometry, free-uptake time, and siRNA stability, but not affected by the antibody target changes and module affinity improvement to siRNA. Overall, our study represents an example of noncovalent ARCs distinct from other antibody–siRNA systems reported so far. Our data implied that this one-to-one pairing mode is promising and may open up new perspectives for antibody–siRNA delivery.

Materials and methods

Cell lines

NCI-N87, SK-OV-3, MDA-MB-453, MCF-7, NCI-H929, A431, and K562 cell lines were maintained in Roswell Park Memorial Institute (RPMI) 1640 medium supplemented with 10% fetal bovine serum (FBS) and 1% penicillin/streptomycin at 37°C in 5% CO_2. HEK 293F cells were a kind gift from Dr F. Long (Wuhan University, China) and maintained in Union-293 expression medium with shaking at a speed of 110 rpm at 37°C in 5% CO_2. RPMI 1640 medium, FBS, and other cell culture supplementary reagents were purchased from Procell, Inc. (Wuhan, China). Union-293 expression medium was purchased from Union-Biotech (Shanghai, China).

SiRNA and its chem score calculation

The siRNA sequences were obtained from reports [4, 24]. The anti-Pten siRNA sequences are as follows: sense, AAGAUGAUGUUUGAAACUAUU; antisense, AAUAGUUUCAAACAUCUUGU. The anti-PPIB siRNA sequences are as follows: sense, ACAGCAAAUUCCAUCGUGUTT; antisense, ACACGAUGGAAUUUGCUGUTT. The anti-Fluc siRNA control (siCtrl) sequences are as follows: sense, CUUACGCUGAGUACUUCGATT; antisense, UCGAAGUACUCAGCGUAAGTT. To conjugate siRNA on biosensors, with sulfo-Cy7 dye or SMs, the 5′ terminus of sense strand was modified by amino-C6 and supplied by the vendor (Biosyntech). The base modification includes 2′-OMe, 2′-F, 2′-H (DNA), (*S*)GNA, and phosphorothioate. The chem score of siRNAs was calculated by counting the modification sites in the sequence. The chemotypes could be the routine Alt OMe, ESC, Adv ESC, and ESC+, which were detailed in the figures and supplementary figures. All the modified siRNA was characterized by ESI-MS. The siRNA strands (200 or 40 μM each) were annealed at sense/antisense molar ratio = 1/1 in the nuclease-free duplex buffer (30 mM HEPES, 100 mM potassium acetate, pH 7.5) to obtain a duplex stock (100 or 20 μM) according to the IDTDNA's protocol. Absence of free single strand was examined by the native polyacrylamide gel electrophoresis comprising 20% acrylamide (sodium dodecyl sulfate free). Both the double and single strands could be visualized by GelRed staining.

DsRBD protein expression and purification

The dsRBDs of RNA helicase A (RHA; NP_001348.2), nuclear factor 90 (NF90; NP_001131145.1), trans-activation response RNA-binding protein 2 (TRBP2; NP_004169.3), Stau1 (NP_001032405.1), adenosine deaminase acting on RNA (ADAR; NP_001102.3), protein activator of the interferon-induced protein kinase (PACT; NP_001132989.1), and protein kinase R (PKR; NP_001129123.1) were back translated into complementary DNA (cDNA; all sequences are available in supplementary information) and synthesized by GenScript (Nanjing, China). The cDNAs were cloned into pET-28a(+) vector. The plasmids were transformed into *Escherichia coli* Rosetta 2(DE3) cells (Millipore, USA). Single clone was picked and grown in Luria-Bertani medium at 37°C until OD_{600} reached at 0.6–0.8. Isopropyl β-D-thiogalactoside

was added to the medium at a final concentration of 1 mM. The temperature of incubator was adjusted to 22°C. The culture was shaken for another 12 h, then harvested and resuspended in lysis buffer (20 mM Tris–HCl, 1 M NaCl, pH 7.2). After French press cell lysis, the soluble lysate was isolated by centrifugation at 10 000 × *g* for 10 min. The his × 6 tagged protein was purified from the supernatant by Ni affinity chromatography, followed by the ion exchange chromatography equipped with HiScreen SP HP column (Cytiva, Catalog 28950515). The ion exchange purification was performed by a gradient elution (0%–100%) of phase A (50 mM MES, pH 6.0) and phase B (50 mM MES, 1M NaCl, pH 6.0), with an elution volume of 30 ml (rate 1 ml/min). The purified dsRBDs were exchanged to phosphate buffered saline (PBS) by Sephadex G-25 desalting column. All proteins were examined by sodium dodecyl sulphate–polyacrylamide gel electrophoresis (SDS–PAGE) and size exclusion chromatography (SEC) and measured at A260/A280 to ensure the absence of fugitive bacterial RNAs [25]. SEC characterization of all antibodies is available in Supplementary Fig. S1. The samples with A260/A280 ratio 0.5–0.7 were accepted for further investigation.

Biolayer interferometry assay

Biolayer interferometry assay (BLI) was performed at 30°C using a ForteBio Octet Red96 biosensor system (ForteBio, Germany) with amine reactive second-generation (AR2G) biosensors. The C6-amine modified siRNA (5′ end of sense strand) was loaded onto the biosensors at a concentration of 1 μM according to the biosensor's loading and quenching protocol. After 3-min wash with PBS to get a smooth baseline, the biosensors were dipped into wells containing various concentrations of proteins (0.5–100 nM in PBS) for 180 s, and followed by a 120-s dissociation in PBS. The siRNA immobilized biosensors can be regenerated for next cycles by washing with glycine regeneration buffer (10 mM glycine–HCl, pH 1.5) for 120 s. The data were analyzed by the ForteBio Data Analysis 11.1 software with a standard 1:1 binding model.

Electrophoretic mobility shift assay

The dsRBDs were incubated with sulfo Cy7-siRNA (2 pmol) for 10 min (dsRBD/siRNA molar ratio of 2:1) at room temperature for complex assembly. The complex was then supplemented with the different sera or competitors for 5 min. The final serum concentration could be 30% or 80% of mouse, bovine, and human sera. The competitors tested in the study include total cellular RNA (10–100 ng/μl), single-stranded RNA (ssRNA; 100 ng/μl), single-stranded DNA (ssDNA; 100 ng/μl), double-stranded DNA (dsDNA; 100 ng/μl), bovine serum albumin (BSA; 1 mg/ml), and heparin (10 ng/μl). The binding stability of dsRBDs with siRNA was verified by electrophoresis in 0.5% agarose gel (100 V, 10 min).

Antibody expression and purification

The bifunctional antibody was constructed using the knob-into-hole technology [26, 27], which renders a typical hole (Y349C, T366S, L368A, Y407V, and F405K) chain and knob (S354C, T366W, and K409A) chains bearing the Stau1 dsRBDs at N-terminus (all sequences are available in supplementary information). The cDNA encoding the chains was cloned into an antibody expression vector pTrioz-hIgG1. The plasmid was then amplified and purified from Top10 strain by Promega Plasmid Maxiprep Kit for transient antibody expression. For transfection, HEK 293F cells were suspended at a density of 1.5×10^6 cells/ml in fresh Union-293 media. To 100 ml of suspension cells, separate dilutions of 125 μg plasmid and 400 μg PEI MAX (Polysciences, Catalog 24765) in 5 ml Opti-MEM, were mixed, incubated at 37°C for 5 min, and added. The transfected culture was returned to the incubator (110 rpm, 37°C, and 5% CO_2). Twenty hours later, the culture was supplemented with sodium butyrate (a final concentration: 10 mM) and glucose (a final concentration: 50 mM). Five days after transfection, the culture was spin down. The supernatant was collected, and the antibody was purified from it by a protein A column (1 ml, Bestchrom) according to the manufacturer's protocol. The protein A elution buffer is 100 mM arginine–HCl, pH 3.0. The bifunctional antibody was further purified by ion exchange chromatography equipped with HiScreen SP HP (Cytiva, Catalog 28950515) column to remove nonspecific bands. The mobile phase composition changes phase A–B (50 mM bicine, pH 8.3) with gradient increase of B (50 mM bicine, 1M NaCl, pH 8.3) from 0% to 100% (v/v). The final antibody samples were measured by the BCA assay and stored at 10 mg/ml in 10% glycerol buffer in PBS for further investigation.

Antibody–siRNA pairing and conjugation

The bifunctional antibody and siRNA were paired at a molar ratio of 1/1 otherwise noted (4/1, 3/1, 2/1, and 0.5/1 in the stoichiometry experiment). The complex (10 μM of siRNA and antibody) was paired in the PBS buffer at room temperature for 5 min, which is sufficient to form stable pair for next investigation. The presence of minimal amount of glycerol (<10%, from the antibody stock) has neglectable effect on the pairing. The formation of antibody–siRNA pair (ratio 1/1) was characterized by electrophoretic mobility shift assay (EMSA) and SEC chromatography (Supplementary Fig. S2). The pair was directly used for *in vitro* cell and animal studies without further purification due to its noncovalent nature. Minimal free siRNA or antibody could coexist but should be <10% in proportion.

The DAR1 species of ARC was obtained according to our previous report [28]. Briefly, a trastuzumab thiomab was expressed and purified as described earlier. After activation of thiomab using a typical reduction/oxidization procedure, antibody (10 mg) and a maleimide-functionalized siRNA were mixed at molar ratio 1/1.2 and incubated at room temperature for 2 h. Then, the DAR1 species was purified from the reaction by a HiScreen Q HP column (Cytiva, Catalog 28950511). The purified ARC-DAR1 was exchanged to PBS by Sephadex G-25 desalting column, and used directly for animal study. The covalent antibody–siRNA pair was synthesized by a similar method to ARC, but the antibody was changed to the mut4 tras bifunctional antibody plus a free cysteine at site 209 (sequence is available in supplementary information).

Zeta potential analysis

For zeta potential measurements, the antibody samples (1 mg/ml in PBS, pH 7.4) were diluted 10 times in MilliQ water, and 700 μl of diluted sample was loaded in a disposable folded capillary cuvette (DTS1070, Malvern Panalytical). Three measurements were performed at intervals of 300 s, and each measurement comprised 20 runs.

Flow cytometry

The flow cytometric assay was used to determine the binding ability of bifunctional antibodies to HER2-positive (HER2+) cell line NCI-N87, epidermal growth factor receptor (EGFR)-positive cell line A431, B cell maturation antigen (BCMA)-positive cell line NCI-H929, and TfR1-positive cell line K562, respectively. Briefly, cells were digested with trypsin (Gibco, Catalog 15050065) and resuspended in RPMI 1640 at density of 25 000 cells per ml. The sulfo Cy5-labeled antibody (∼1 dye per antibody) or antibody–siRNA pair (Cy5 is labeled at the sense strand of siRNA) was added at a final concentration of 50 nM. After 1-h incubation on ice, cells were washed twice and resuspended in PBS, the fluorescent intensity of cells was analyzed by CytoFlex S (Beckman, USA) according to the manufacturer's instructions. All data were triplicate and processed by FlowJo 10.6.2 for interpretation.

In vitro gene silencing assay

In this, 10 000 cells were seeded into 96 well plates 1 day before experiments. On the next day, antibody–siRNA pairs were prepared by incubation of antibody/siRNA (molar ratio = 1/1) at room temperature for 5 min and added to cells at the indicated concentrations (200 nM or a series of dilutions from 400 to 1 nM). Seventy two hours later, cells were harvested and total RNA was isolated using the total RNA extraction reagent Trizol (Vazyme, R401-01) according to the manufacturer's instruction. Real time RT-qPCR was performed with the HiScript II One Step qRT-PCR SYBR Green Kit (Vazyme, Q221-01) on CFX Connect™ RT-qPCR detection system (Bio-Rad, USA). The data were analyzed with Bio-Rad CFX Maestro 1.1, and relative mRNA change in PLK1, PTEN, CTNNB1, and PPIB were calculated by referring to the housekeeping gene β-actin according to the $2^{-\Delta\Delta CT}$ algorithm. The primers for RT-qPCR are listed as follows: β-actin forward: 5′-CCTGTACGCCAACACAGTGC-3′, β-actin reverse: 5′-ATACTCCTGCTTGCTGATCC-3′; PTEN forward: 5′-TCCCAGACATGACAGCCATC-3′, PTEN reverse: 5′-TGCTTTGAATCCAAAAACCTTACT-3′. The firefly luciferase (Fluc) siRNA was used as the siCtrl. In some experiments, other negative control groups, such as untreated blank cells, siRNA alone (200 nM), and antibody alone (200 nM), were also designed. The lipopfectamine RNAiMAX (lipo)-transfected siRNA groups (5 nM) were established as positive controls to confirm the potency of siRNAs.

SM enhancer synthesis and siRNA conjugation

SM enhancers were synthesized by coupling the SMs with a short PEG2-acid linker. The acid group was then activated with the N-hydroxysuccinimide (NHS) ester and then conjugated with the 5′ amino end of siRNA sense strand. The siRNA strand was purified by reversed-phase High Performance Liquid Chromatography (HPLC) and annealed with the antisense strand to form a duplex. The detailed synthesis procedures and product characterization are provided in the supplementary information.

Confocal imaging

NCI-N87 cells (20 000 cells) were seeded in confocal dishes (3.5 cm) and cultured overnight. After wash of monolayer by RPMI 1640 once, antibody and siRNA (labeled with sulfo Cy5 at the antisense strand of siRNA) were paired as described earlier and added into dishes at the concentration of 50 nM in RPMI 1640. Dishes were returned to cell culture incubator at 37°C in 5% CO_2 for 24 h. Cell membrane and lysosome were then stained with Wheat Germ Agglutinin (WGA) Alexa Fluor 594 (5 nM, Invitrogen, W11262) and Lyso-Tracker Green (100 nM, Beyotime, C1047S) for 5 min, respectively. Cells were washed twice with PBS and imaged with confocal laser scanning microscopy (Leica, USA).

Arginine scanning mutagenesis

The crystal structure of Stau1 dsRBD/dsRNA complex (PDB ID: 6htu) was used as the template model for *in silico*-guided mutagenesis. The single-point mutation is introduced in the dsRBD3 (aa11–82) and dsRBD4 domains (aa113–184), respectively. It finally generates a total of 135 individual models by mutagenesis wizard of UCSF Chimera v1.19. To predict the interaction potential with siRNA, we measured the distance between the mutated arginine residue (guanidine head) and the nearest phosphate group in siRNA by the PyMol measurement wizard. The candidate residues with an ion-pair distance <5 Å were selected for arginine scanning mutagenesis. We selected 13 single-position mutants in dsRBD3 and 11 mutants in dsRBD4 for the wet bench screening. The mutation position was introduced into the pET-28a(+) expression vector by site-directed mutagenesis according to kit protocol (Vazyme, C214-01). The Stau1 dsRBD protein mutant was purified as aforementioned. The affinity to siRNA was measured by BLI for each clone. The arginine-mutated bifunctional antibody was generated with knob-into-hole technology, purified with protein A and HiScreen SP HP column as mentioned previously.

Calculation of net protein charge

Sequence-dependent net charge at pH 7.4 was calculated using the ProtPI Protein Tool (https://www.protpi.ch/Calculator/ProteinTool). The calculation only covers the Stau1 domain and thus the whole protein is a single-chain peptide, which can fit the algorithm. All cysteines were assumed to form disulfide bridges. The N-terminal amine and C-terminal carboxylic acid were assumed to be neutralized and not counted at calculation.

Western blotting

NCI-N87 cells were seeded into 12 well plates (50 000 cells per well) 1 day before the experiment. Antibody–siRNA pair was added to the complete growth media of cells at the final concentrations of 20 and 200 nM, respectively. Cells were incubated for 72 h. Cell protein was extracted by RIPA cell lysis buffer (Beyotime, P0013J). The concentration of total protein was quantified by Pierce™ BCA Protein Assay Kit (Thermo Scientific™, 23225). Samples (10 μg) were loaded into wells of 4%–20% SDS–PAGE gel (ACE Biotechnology, ET12420Gel) and electrophoresed at 120 V for 2 h. The protein on gel was transferred to immobilon P PVDF membrane (Millipore, IPVH00010), and then blocked with 3% (w/v) BSA for 2 h at room temperature, followed by incubating with primary antibody (anti-Pten monoclonal antibody, Cell Signal Technology, #9559, 1:1000; β-Actin Mouse mAb, ABclonal, AC004, 1:5000) at room temperature for 1 h, and secondary antibody [horseradish peroxidase (HRP)-conjugated Goat anti-Rabbit IgG (H + L), Proteintech, SA00001-2, 1:5000; HRP-conjugated Goat anti-Mouse IgG (H + L), ABclonal, AS003,

1:5000] at room temperature for 1 h. After three-time washes with TBST buffer (10 mM Tris.HCl, 150 mM NaCl, 0.05% Tween-20, pH 7.5), enhanced chemiluminescent HRP substrate (Proteintech, Catalog PK10001) was added and chemiluminescence was detected using the ChemiDoc XRS + Gel Imaging System (Bio-Rad).

Pharmacokinetic study

All animal studies were performed under the protocol approved by the Institutional Animal Care and Use Committee of Wuhan University, in accordance with the guidelines of the Chinese Regulations for the Administration of Affairs Concerning Experimental Animals. To study the pharmacokinetics, 1 mg of anti-Pten siRNA (adv ESC) was paired with 11 mg Tras antibody for 5 min and intravenously injected to BALB/c male mice. A total of 10 μl of blood samples was collected at indicated time points (10 min, 1 h, 3 h, 6 h, and 9 h). The blood samples were diluted by 20 μl of PBS. The supernatant after spin down was collected and stored at −80°C until the stem-loop polymerase chain reaction analysis. For covalent pair and ARC DAR1, equivalent amount of siRNA (1 mg) was injected via tail veins but the blood collection time points were extended to 5 days (12, 24, 48, 72, 96, and 120 h). To quantify the siRNA remaining in blood, an stem-loop RT-qPCR assay was developed according to reports [29, 30]. Briefly, 1 μl of siRNA fraction solution (from supernation) was aliquot for stem-loop reverse transcription (RT; MR101, Vazyme), followed by real time qPCR quantification using the AceQ qPCR Probe Master Mix (Vazyme, Q112). The measured CT (Cycle Threshold) values were then applied to a standard curve to determine the corresponding siRNA concentrations. Custom DNA forward primers, reverse primers, RT primers, and TaqMan probes were all obtained from Sangon Biotech (Shanghai, China). Their sequences are available in Supplementary Table S1.

Statistical analysis

Statistical analysis was performed using GraphPad Prism 9.3.0, data were presented as mean ± standard deviation, *P*-values were calculated using the two-way analysis of variance with Tukey's multiple comparison test, and $P < 0.05$ was considered to be statistically significant.

Results

Stau1 dsRBD34 is a reliable siRNA recruiter

The dsRBDs are highly specialized domains found in a wide variety of dsRBPs in prokaryotic and eukaryotic cells. They might be present as multiple copies in a single protein, but each copy is heterogeneous from the others in sequence [31]. Besides sequence, these dsRBDs are differentiated in many aspects, including substructure, linker length, affinity, and selectivity [32], which makes the dsRBPs bearing them extremely diverse in function and activity [33]. To identify a reliable siRNA recruiter for antibody modularization, we first screened the tandem domains from seven human dsRBPs (Fig. 1A), including RHA, TRBP2, NF90, Stau1, ADAR1, PACT, and PKR. These proteins were chosen because they all possess tandem dsRBDs in one molecule. Multiple domains can tether together to create a much larger binding interface that recognizes a longer sequence and produces a higher affinity [34]. The relevant domains were cloned, expressed, and purified using the recombinant protein technology (Supplementary Fig. S3). Despite the variety in molecular weights, most dsRBDs display the dissociation constant (K_D) values in the low nanomolar range (Fig. 1B and Supplementary Fig. S4).

We found that the avidity of all dsRBDs to siRNAs was highly stable in PBS buffer, but a discrepancy can be observed when the complex was co-incubated with sera (mouse serum, FBS, and human serum). More specifically, dsRBDs from RHA, NF90, and Stau1 demonstrated the highest binding stability with siRNAs than all others (Fig. 1C and Supplementary Fig. S5). We then evaluated the releasability of siRNA from dsRBD/siRNA complexes by competing with the isolated cellular total RNAs (100 ng/μl), which mimics the release process in cytosols once dsRBD/siRNA complex being delivered to cells [23]. The complexes from all the dsRBDs can be disassembled to release the free siRNA by cellular total RNAs, with the exception of dsRBDs from TRBP2 and NF90. The result is a little surprising, because all dsRBDs show homology in sequences and topological structures (Fig. 1D). When the unstructured linker sequences between domains were aligned (Supplementary Table S2), we found that TRBP2 and NF90 have many more hydrophobic residues (rich in A, V, L, and P) in the linker loops, which might cause the poor response to RNA displacement. Accordingly, Stau1 dsRBD34 was selected as the candidate for further evaluation owing to its high affinity, specificity, and binding stability.

Stau1 is a regulatory protein that mediates in the transport, translation, and decay of mammalian mRNAs [35]. It contains four dsRBDs, but only dsRBD3 and dsRBD4 can adopt the canonical αββββα fold for siRNA recognition [35]. These two dsRBDs work in tandem to establish the surface contact to two minor grooves (r1 and r2) and one major groove (r3) on the siRNA separately (Fig. 2A) [36]. Despite sequence independence, we were worried that RNA recognition by Stau1 dsRBD34 might be sensitive to the chemical modification on siRNA bases, because it was reported that many dsRBPs cannot bind with the ribonucleotide analogues such as DNA, PNA, or PMO [37]. As well known, U.S. Food and Drug Administration (FDA)-approved siRNA drugs are all heavily modified to increase the stability of siRNAs [38]. In order to investigate whether siRNA modification impairs the binding avidity, we immobilized siRNAs of six chemotypes on AR2G biosensors and measured the K_D values to Stau1 dsRBD34 by the Octet BLI assay (BLI traces are available in Supplementary Fig. S6). As shown in Fig. 2B, the binding was not affected by most chemotypes, with the exception of hybrid mode which contains a DNA sense strand. To further explore the selectivity of Stau1 dsRBD34 to siRNA, we utilized dsRBD34 to recruit siRNAs in the presence of other competitors such as cellular total RNAs, ssRNA, ssDNA, dsDNA, BSA protein, and heparin sodium (Fig. 2C). The recognition of siRNA by Stau1 dsRBD34 was highly specific, and only interrupted by cellular RNAs at high concentrations. At an RNA concentration of 50 ng/μl, the dsRBD/siRNA complex was disrupted totally and instantly (Fig. 2D). We also found that the interaction between Stau1 dsRBD34 and siRNA is insensitive to acidic conditions (pH 4.5–7.4), indicating that the complex might be stable in the endosomal compartment (Fig. 2E). Altogether, these data demonstrated that Stau1 dsRBD34 is a potent and selective siRNA binder, which would be reliable as a module for antibody construction.

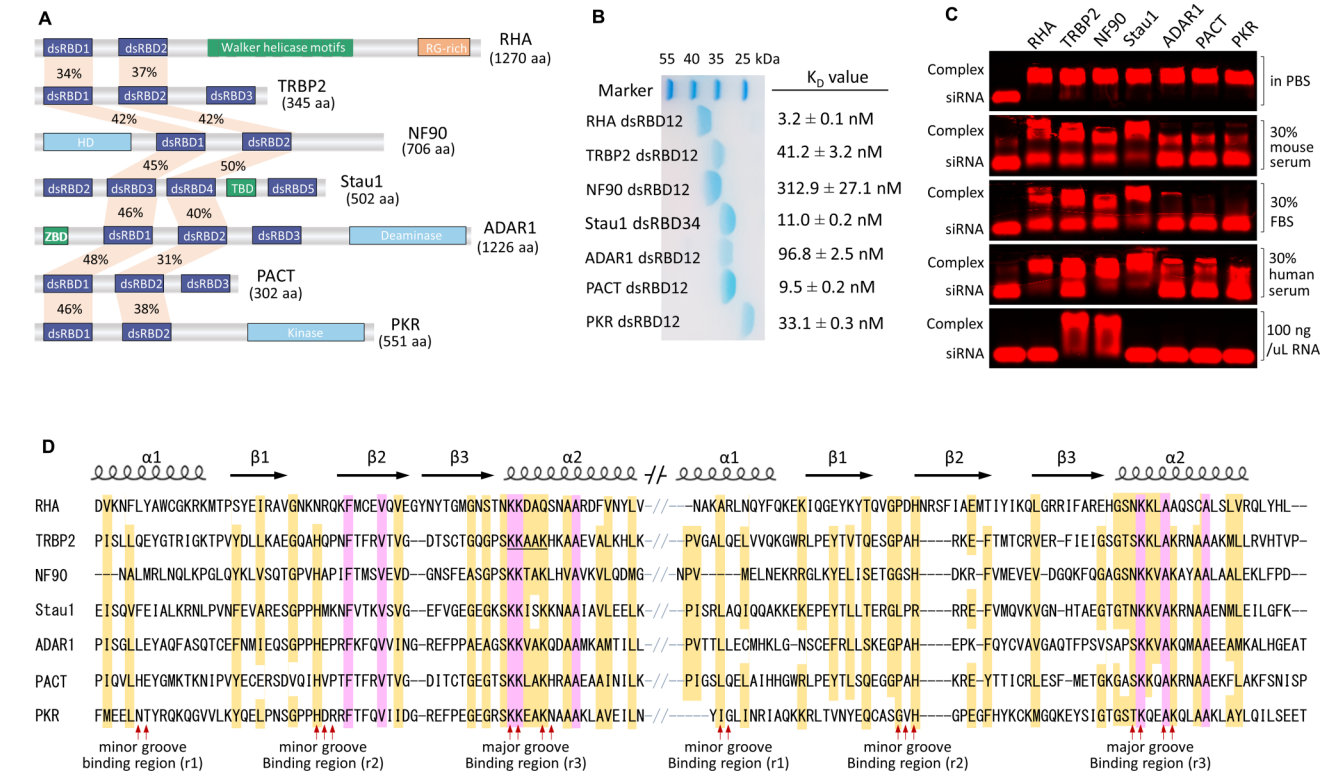

Figure 1. The parallel comparison of dsRBDs from seven human dsRBPs. (**A**) Schematic representation of the domain architectures of seven RNA-binding proteins. Percentage similarity between domains is indicated. (**B**) SDS–PAGE analysis and BLI assay to determine affinity against siRNA duplexes [wild type (WT)]. (**C**) The binding stability of dsRBD/siRNA complexes (10 fmol per well) in the presence of PBS buffer, sera (30%), and competitive RNAs (100 ng/μl of total cellular RNA). (**D**) Sequence alignment of $\alpha\beta\beta\beta\alpha$ regions of seven dsRBD proteins. Identical and similar residues are shaded in pink and yellow, respectively. The red arrows indicate the critical residues involved in protein–RNA interactions. The secondary structure elements are shown above the sequence.

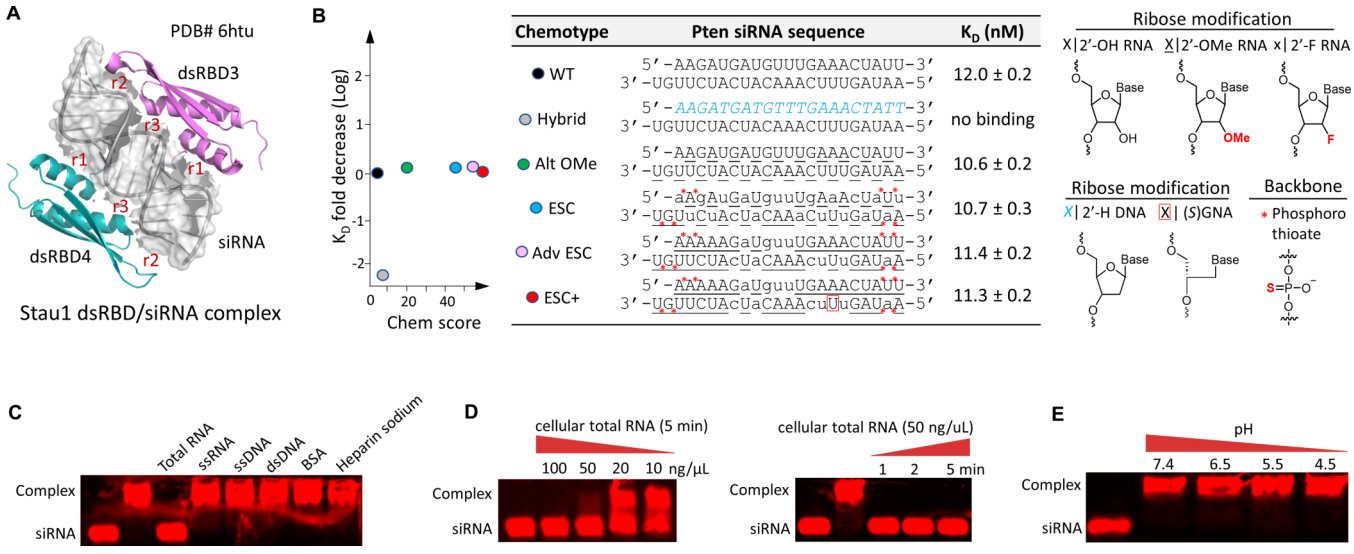

Figure 2. Characterization of Stau1 dsRBD34 in siRNA recruiting. (**A**) Structure of Stau1 dsRBD34 in complex with siRNA. (**B**) Evaluating the binding affinity of dsRBD34 to siRNAs of different chemotypes. Chem score was used to scale the modification intensity. (**C**) siRNA displacement challenged by oligoes (100 ng/μl), BSA protein (1 mg/ml), and anionic heparin polymer (10 ng/μl). (**D**) Competitive test of dsRBD34/siRNA complex by cellular total RNA with either different concentrations or time intervals. (**E**) The pH sensitivity of dsRBD34/siRNA assembly.

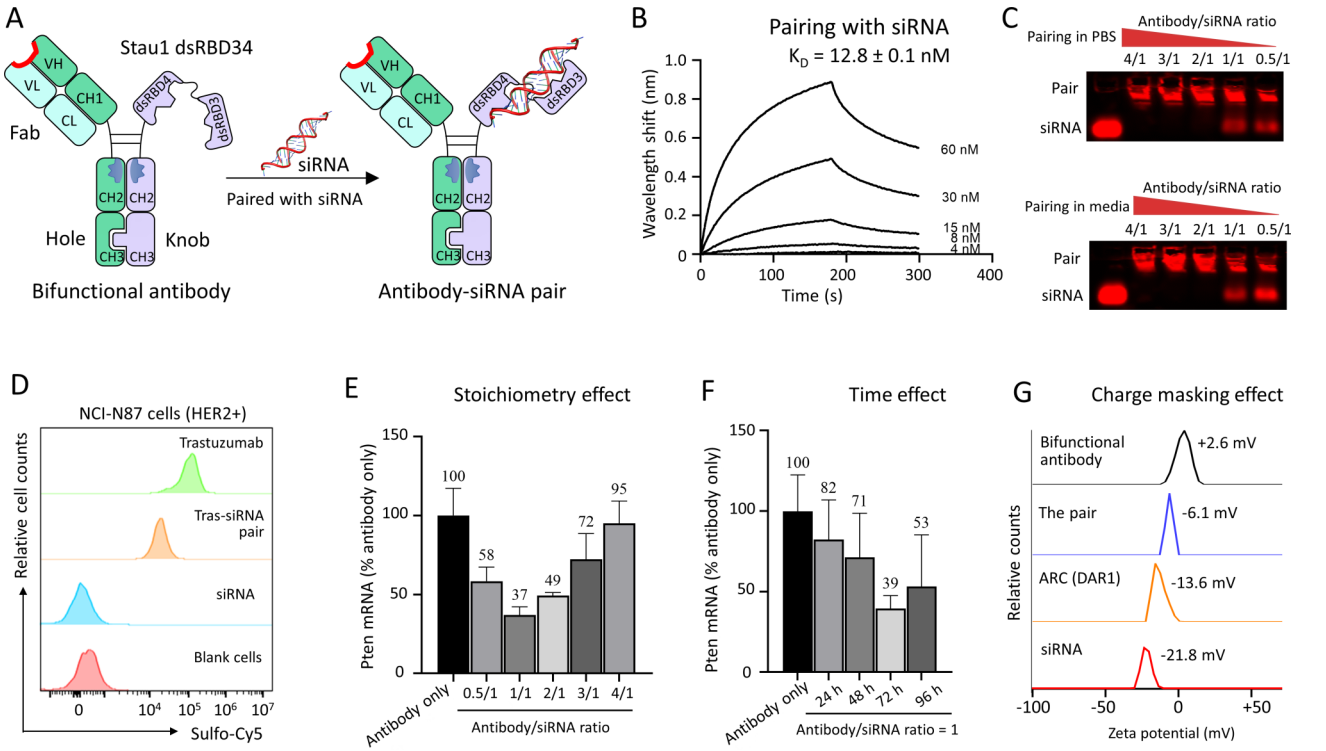

Figure 3. Stau1 dsRBD34 as a module to replace one Fab arm of antibody for siRNA pairing and delivery. (**A**) The structural scheme of a "knob-into-hole" bifunctional antibody and its pair with siRNA to form one-to-one diligent complex.(**B**) Association and dissociation kinetics of the immobilized ESC siRNA against antibody titrated from 4 to 60 nM, revealing the $K_{on} = 3.42 \times 10^5$ M^{-1} s^{-1}, $K_{off} = 4.36 \times 10^{-3}$ s^{-1}, and $K_D = 12.8 \pm 0.1$ nM by BLI. (**C**) Stoichiometry and titration of antibody–siRNA complexation in PBS or RPMI 1640 media by gel mobility shift assay. (**D**) Anti-HER2 binding test (50 nM) on NCI-N87 cells by flow cytometry. (**E–G**) The antibody–siRNA pairs (200 nM siRNA equivalent) exhibit a stoichiometric and time effect in mRNA silencing, and a masking effect to siRNA charges.

Stau1 dsRBD34 as a module for antibody–siRNA pairing and delivery

The Stau1 dsRBD34 was engineered into the N-terminus of one heavy chain to replace the position of Fab domain. As shown in Fig. 3A, the resulting construct is assembled into a bifunctional antibody via a knob-in-hole technology. Once mixed with siRNA, the dsRBD recruits one molecule of siRNA and forms a diligent one-to-one antibody–siRNA pair, which is structurally equivalent to the DAR1 ARC species but noncovalently conjugated. To investigate whether the steric hindrance from antibody domains would negatively impact the siRNA recruitment, we assessed the binding affinity of bifunctional antibody to the WT siRNA by BLI. As shown in Fig. 3B, its K_D value to siRNA is comparable to that of the free Stau1 dsRBD34 ($K_D = 12.8 \pm 0.1$ nM). The traces of binding kinetics include a fast association ($K_{on} = 3.42 \times 10^5$ M^{-1} s^{-1}) and slow dissociation ($K_{off} = 4.36 \times 10^{-3}$ s^{-1}) rate, indicating a high degree of siRNA occupancy. Despite a high affinity, an incomplete recruitment of siRNA to some degree was observed at the molar ratio 1/1 in the gel mobility shift test (Fig. 3C). Further increase of the titration ratio (4/1, 3/1, and 2/1) can completely sequester the free siRNA. This result demonstrates that the recruitment at ratio 1/1 is not exhaustive. Nevertheless, the pair of trastuzumab (tras) and siRNA (sulfo-Cy5 labeled) at this ratio can remarkably shift the HER2+ NCI-N87 cells to the right in the flow cytometry (Fig. 3D), indicating a successful siRNA pairing and good delivery ability of bifunctional antibodies.

To assess the gene silencing activity, an anti-Pten siRNA (adv ESC) was paired with anti-HER2 bifunctional antibody (Tras) and delivered to NCI-N87 cells at varying antibody/siRNA ratios by free uptake. A stoichiometry effect was seen in Fig. 3E. The best activity was observed at an antibody/siRNA ratio of 1/1, but not at higher or lower ratios. It is because there is plenty of residue antibody (without siRNA paired) or free siRNA after pairing at these inadequate ratios, which can compete with the pair to bind cells and reduce siRNA delivery efficiency. Therefore, a purification process after antibody–siRNA pairing could maximize the therapeutic effect. However, as a noncovalent system, dissociation is a concern, especially in the organic solvent, high salt or other purification conditions. So far, we lack a dedicated method to purify the pair, but we can analyze the formulation by EMSA assay or SEC to make sure the dominance of pair in composition (>90%). Besides the stoichiometry, the uptake interval (Fig. 3F) and siRNA modification chemistry (Supplementary Fig. S7) also affect the Pten knockdown efficiency, which is in agree with our previous report that siRNA stability is the rate-limiting factor of ARC bioactivity *in vitro* [28].

It was interesting to find that dsRBDs can mask the siRNA charges after the pairing (Fig. 3G). The charge masking effect could be attributed to not only the siRNA surface shielding by Stau1 module but also the charge neutralization by positive residues (K, R, and H) in the r1–3 binding regions. The electrostatic status of antibodies is a key factor in

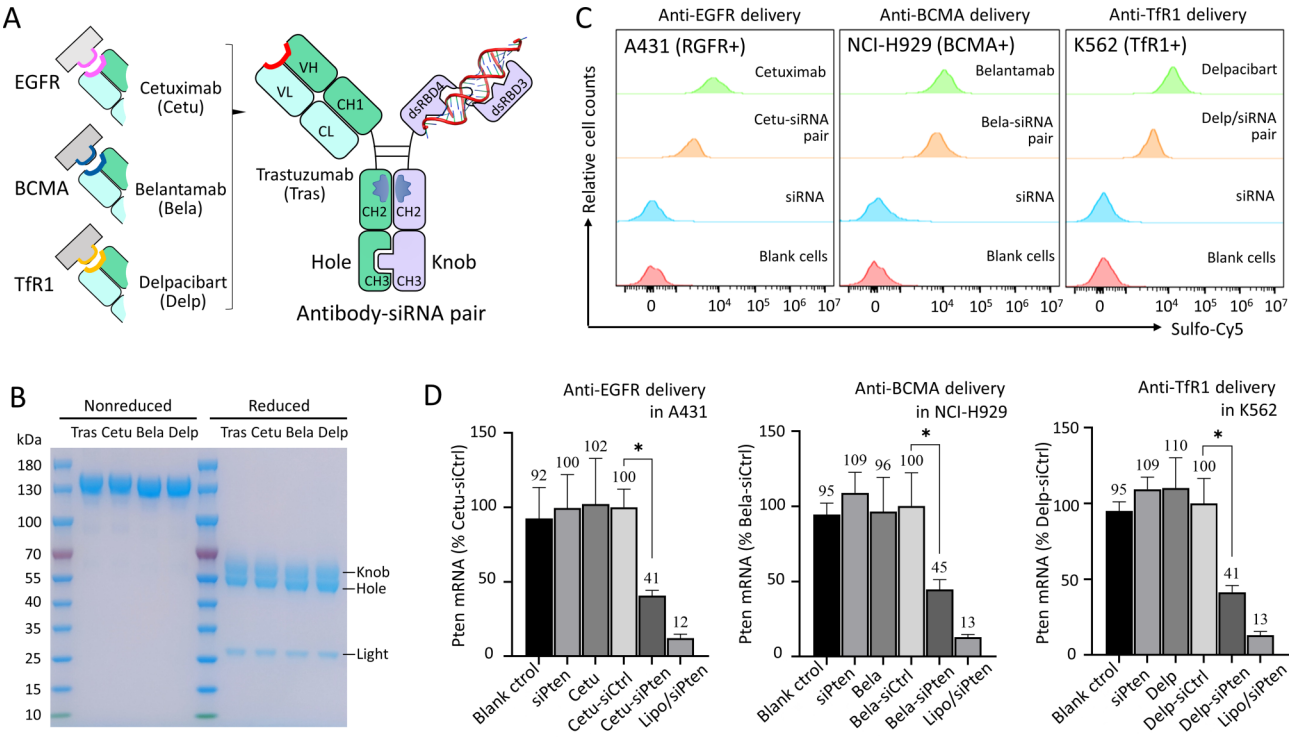

Figure 4. Modular design of bifunctional antibodies across multiple target antigens. (**A**) Scheme of antibody–siRNA pairs engineered from anti-EGFR Cetu, anti-BCMA Bela, and anti-TfR1 Delp antibodies. (**B**) SDS–PAGE analysis to profile the hole heavy, knob heavy, and light chains of four bifunctional antibodies. (**C**) Flow cytometry charts showing the binding capability of antibodies (50 nM) to the corresponding antigen-positive cells. (**D**) Gene silencing activities of antibody–siRNA pairs in comparison to the negative (blank, siRNA, or antibody only) and positive (lipo transfection) controls. All the drugs or vehicles were applied on cells by 72-h free uptake at the concentration of 200 nM, with an exemption of lipo/siPten group which was transfected at 5 nM owing to the high efficiency of lipofectamine RNAiMAX. ∗, $P < 0.05$.

determining the circulatory half-life *in vivo* [6]. For example, DAR1 ARC, displaying zeta potential over −10 mV, has a circulatory half-life of only ∼6 h [5], which is much shorter than the charge-neutral Tras antibody ($t_{1/2}$ > 72 h) in mice. The mechanism of its fast clearance is poorly understood, but increasing evidences indicated that it links to the payload's negative charges which can induce nonspecific protein binding and cell retention [39, 40]. The charge masking effect we observed on antibody–siRNA pairing system might be beneficial to the *in vivo* application.

Expansion of the addressable targets and cells

To demonstrate the generality of the pairing platform in siRNA delivery, we tried to target other tumor cell antigens by exchanging the variable regions (VH and VL) of bifunctional Tras antibody with cetuximab (Cetu), belantamab (Bela), and delpacibart (Delp) sequences, which can recognize the EGFR, BCMA, and the TfR1, respectively (Fig. 4A). The three new constructs worked well in antibody assembly, expression, and purification (Fig. 4B). All of them demonstrated the good selectivity and affinity to the target cells (Fig. 4C). Similar to anti-HER2 Tras antibody, the siRNA pairs with new antibodies led to significant knockdown of Pten mRNA in the corresponding cells (Fig. 4D). Notably, treatment by siRNA pairs resulted in a gene knockdown effect that correlates with antigen-expression status of cells (Supplementary Fig. S8). Together, these results demonstrated the potential of using the pairing platform to target multiple clinic-relevant antigens and cells.

Endosome-to-cytosol import by conjugating SM enhancers

Having demonstrated the expandability of the pairing platform to multiple cells and targets, we investigated whether we could enhance the gene silencing activity without using cationic assistance. In the aforementioned test was applied the high concentration of ARCs (200 nM), partly owing to the rate-limiting step of endosome-to-cytosol import after endocytosis by free uptake [3]. We sought to explore whether the RNAi potency could be improved by conjugating siRNA with SM enhancers to facilitate the import (Fig. 5A). Small organic molecules, such as GalNAc, cholesterol, and fatty acids, have been successfully used to conjugate with siRNA for the purposes of targeting, hydrophobic modulation, or pathway hijacking. Several GalNAc–siRNA conjugates have been approved by the FDA for liver diseases [41].

Here, we selected six SMs, either natural components or lysosomotropic drugs, to append on the 5′ end of sense strands of siRNAs (Fig. 5B). After pairing with the anti-HER2 Tras antibody, we screened the chemical conjugates by assessing the improvement of RNAi activity compared with the regular antibody–siRNA pairs in NCI-N87 cells. Of the six candidates, we identified two SM enhancers—prazosin and guanabenz, which show significant enhancement of RNAi potency (Fig. 5C). We then chose prazosin–siRNA conjugate for further evaluation. It was selected because of its neutral charge and no aggregation tendency with siRNA. By pairing prazosin–siRNA with Tras antibody, we evaluated the efficiency of Pten silencing at a series of concentrations

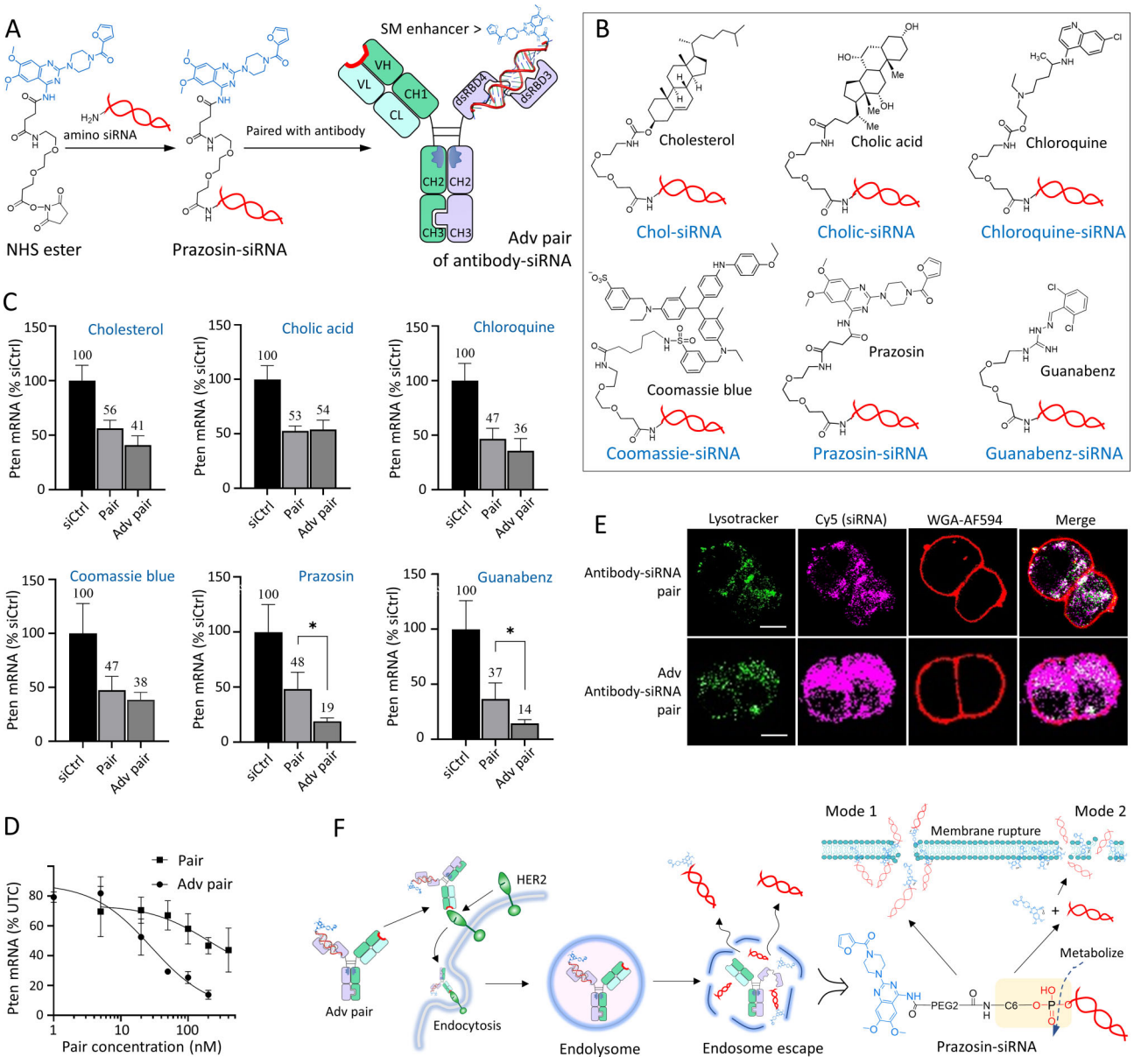

Figure 5. Conjugation with SM enhancer promotes the endosome-to-cytosol import and RNAi activity. (**A**) Step-by-step scheme showing the siRNA conjugation and advanced (Adv) pair formation with the bifunctional antibody. SM enhancer prazosin is used as an example in the scheme. (**B**) Chemical structures of SM enhancers appending to siRNAs. (**C**) RT-qPCR assay to compare the RNAi potency of antibody–siRNA pairs with and without SM conjugation (200 nM; 72 h). ∗, $P < 0.05$. (**D**) The dose-response curves showing a seven-fold discrimination on IC_{50} values between the pair and adv pair. The titration covers wide-range concentrations from 1 to 400 nM. UTC, untreated cell. (**E**) Confocal imaging to track the dislocation of the adv pairs from endosome/lysosome compartments. Scale bar, 10 μm. (**F**) A diagraph illustrating the proposed modes of endosome-to-cytosol import by siRNA-conjugated prazosin.

(Supplementary Fig. S9) and probed the IC_{50} value. As shown in Fig. 5D, this advanced pair exhibited potent target gene silencing and demonstrated ∼7-fold decrease of IC_{50} value in RNAi (from 200 to 28 nM) compared with the pair without prazosin conjugation. In the concentration ranges we titrated, prazosin is biologically inert and induces neither cytotoxicity nor transcriptional misregulation to cells (Supplementary Fig. S10). The result indicates that prazosin can increase the endosome-to-cytosol import of siRNA and improve the delivery efficiency.

To understand the mechanism of endosome-to-cytosol import by SM enhancers, we labeled the endosomal system and tracked the subcellular distribution of siRNAs. As seen in Fig. 5E, incorporation of prazosin has little effect on the organization of endosomal compartments, neither on the appearance nor on the number of these acidic vesicles. The endosome/lysosome vesicles were all diffusely distributed in cells, but a significant translocation of siRNAs outside the endosome/lysosome compartment was observed, despite most siRNAs remain in endosomes. Quantification of the colocalization confirmed that prazosin conjugation led to a significant reduction in colocalization of Cy5-siRNA with Lyso-Tracker Green (Supplementary Fig. S11). Kozik *et al.* reported that prazosin is a lysomotropic compound that promotes the membrane permeation and endosome release [42]. In this study, we envisioned that prazosin was trafficked into endosomes along

with the pairs via receptor-mediated endocytosis (Fig. 5F). Once acidification inside endosomes, the amino atoms of prazosin might be protonated and destabilize the membrane either as the prazosin–siRNA conjugate (mode 1) or free prazosin (mode 2). The latter might play the major role, considering the fast hydrolysis of phosphate diester linkages in endosomes [43].

In silico-guided affinity maturation for activity optimization

The SM appendage yields an advanced antibody–siRNA pair with more potent silencing *in vitro*, we then started to evaluate whether higher affinity to siRNA would continually lead to stronger silencing. As shown in Fig. 6, we focused on increasing the affinity by an *in silico*-guided arginine substitution to find key positions essential for siRNA recognition at the dsRBD/siRNA interface. We herein referred it as an arginine-scanning approach to resemble the well-known alanine-scanning mutagenesis in chemical biology. The rationale of arginine scanning for affinity maturation stems from the previous report that substitution by positively charged aa like arginine (R) or lysine (K) contributes the most to the affinity improvement of siRNA-binding viral protein p19 in the yeast display [25], likely owing to their salt–bridge interaction with siRNA backbones. Encouraged by this discovery, we applied arginine substitution on every aa position of Stau1 dsRBD3 (aa 11–82 in Fig. 6A) and dsRBD4 (aa 113–184 in Fig. 6A) using the mutagenesis wizard of UCSF Chimera v1.19, and generated 135 protein models based on the crystal structure of Stau1 template (PDB code 6htu). The distance from each mutation site (more specifically, the positively charged guanidino head of arginine) to the phosphate of siRNA backbones was measured and plotted against the residue number (#) to generate a topographic map shown in Fig. 6B. The mutagenesis with potential to form stable salt bridges (ion-pair distance < 5 Å) was selected and marked in green. Interestingly, position analysis of these green residues revealed a convergence at regions r1–3, which is in agreement with the reports that grooves of siRNA duplex are the major binding interface with dsRBDs [44].

To validate the prediction, all of these 24 clones were expressed, purified, and profiled against siRNA (Adv ESC) to determine the affinity values (K_D) by the Octet BLI assay (BLI traces are available in Supplementary Figs S12 and S13). The two-dimensional arrays of scanning data in Fig. 6C revealed that most these *in silico*-guided mutagenesis have negligible impact on affinity, but three clones (F45R in dsRBD3; Y134R and G163R in dsRBD4) emerged from the 24-membered library, showing (3–6)-fold improvement of affinity separately. Interestingly, the candidate Y134R site is located outside of r1–3 regions, suggesting that this mutated arginine may interact with phosphates beyond the major/minor grooves of siRNA. To obtain a candidate of maximal affinity, clones containing combinations of the aforementioned mutations were expressed and investigated (Fig. 6D). Surprisingly, the clone mut2, which contains only two mutation sites (F45R and G163R), outperformed the mutant of all three-site combination (mut3), showing a 12.8-fold improvement of affinity ($K_D = 1.0 \pm 0.1$ nM). This clone was further pursued by a supplement of mutagenesis at aa positions of the linker loop, a region located between dsRBDs. It is unstructured and has no interaction with siRNA, which allows the mutagenesis randomly without worrying about protein misfolding. As shown in Fig. 6D, the hydrophobic or negatively charged residues in the loop sequence were selected and substituted by arginine (V90R, I101R, V102R, Q105R, T106R, and E109R), with an assumption of more net positive charges to neutralize siRNA. It was interesting to find that mutations at V90R and V102R, although they are not involved in binding, can improve the affinity ($K_D = 0.4 \pm 0.1$ nM). The clone with mutations at all six selected residues (clone mut8) slightly lost its affinity and showed a K_D value comparable to the WT (Supplementary Fig. S14). Despite the highest net charge value at pH 7.4 (+22.4 mV), this clone was not pursued further.

The candidate Stau1 sequence selected for antibody expression contains two substitutions at dsRBDs (F45R and G163R) and the linker loop (V90R and V102R), respectively. The new modular antibody (mut4 antibody) was then paired with anti-Pten siRNA or prazosin–siRNA and delivered to NCI-N87 cells by free uptake. The gene silencing result in Fig. 7A showed that both pairs can induce significant gene knockdown at all tested concentrations, so does a knockdown effect in protein level (Fig. 7B). However, the augment was not prominent when compared with the WT pair. Altogether, arginine-scanning substitution enabled the affinity maturation, but high-affinity recruiters cannot improve the gene silencing effect *in vitro*.

Pharmacokinetic alteration associates with competition from plasma GAGs

We then investigated the pharmacokinetics of pairs in BALB/c mice and compared it with the canonical DAR1 ARC. The DAR1 ARC was prepared by a thiomab approach we reported previously [25]. Surprisingly, siRNA delivered by mut4 pair quickly disappeared from the blood circulation (Fig. 8A). Its half-life is even much shorter than the DAR1 ARC, albeit its appealing feature of less charges. To figure out the reason, we compared the blood retention profiles of human IgG1 control and bifunctional antibody (without siRNA pairing) in mice. The result in Supplementary Fig. S15 reveals that bifunctional scaffold has neglectable impact on pharmacokinetics and both structures show a comparable long-circulation profile *in vivo*. We speculated that the short retention of siRNA in blood is attributed to the premature dissociation of siRNA from Stau1 dsRBD34 domain. The pair stability was then investigated in 30% and 80% mouse plasma to better mimic the *in vivo* conditions. A significant portion of pairs was dissociated along with the incubation time in 30% or 80% mouse plasma at 37°C. The result is disappointing, but we found that the high-affinity mutation does increase the stability of pair in mouse plasma when compared with the WT pair (Fig. 8B). We then tested another well-known siRNA-binding protein p19, whose avidity to siRNA is much stronger than the mut4 domain (K_D by BLI: 4 versus 400 pM) according to Yang *et al.*'s report [25]. Encouragingly, the pairing between p19 and siRNA is very stable in mouse plasma, as shown in Fig. 8B. Most p19–siRNA pairs remain intact 24 h after a 37-°C incubation in 30% plasma and 12 h in 80% plasma. The result indicates that an ultrahigh-affinity dsRBD34 is required for pair survival in blood, and so on the *in vivo* evaluation of bifunctional antibody strategy in siRNA delivery. Due to the complexity of affinity maturation, further optimization is not pursued in this study. Instead, we engineered a covalent pair to explore the potential of dsRBD masking effect in

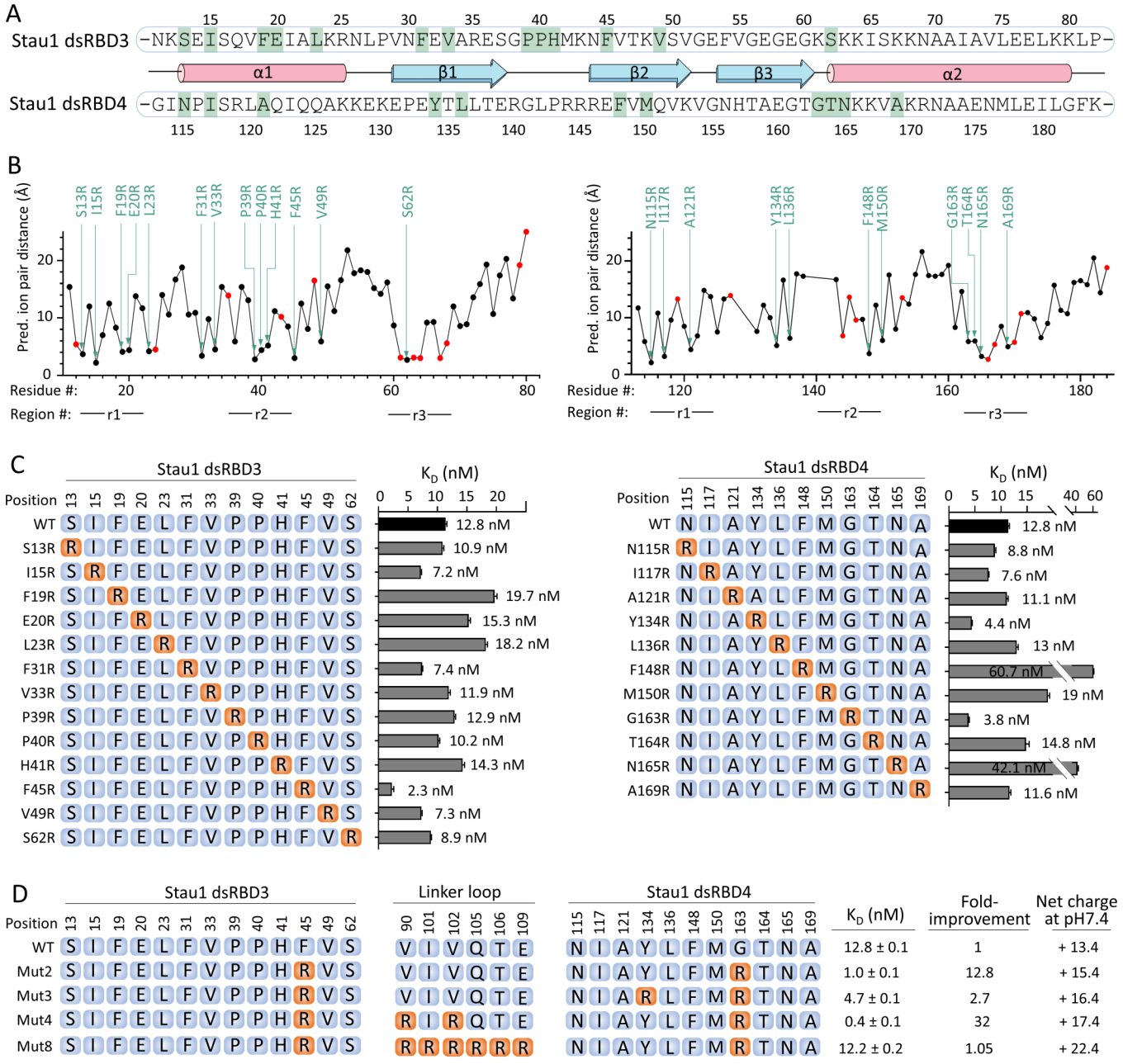

Figure 6. *In silico*-guided arginine scanning to augment the siRNA-binding affinity. (**A**) The aa sequences of Stau1 that were engaged in *in silico* mutagenesis. The residues shallowed in green are selected for mutant cloning. (**B**) A topographic map showing the ion-pair distance from the mutated position (cationic guanidine head) to the nearest siRNA phosphate. The prediction was calculated on the mutagenesis of protein models from template PDB 6htu. The candidate positions with the shortest distance (<5 Å) are labeled in green. The black dots show the arginine mutation, whereas the red ones indicate positions with WT lysine or arginine. (**C**) Arginine scanning of candidate residues to identify essential positions on dsRBD3 and dsRBD4 with affinity augmentation. The K_D values of mutants were measured by the BLI assay with immobilized siRNA (adv ESC). (**D**) Combination of multiple mutated sites on dsRBDs and linker loop to yield an affinity-matured clone with 32-fold improvement. The number in the clone's name indicates the total sites of mutation.

pharmacokinetics. The covalent pair was designed by introducing a Cys mutation at 209 position of knob chain (hinge region). SiRNA was tethered to this position by thiol–maleimide reaction and paired by dsRBD domain owing to the proximity. As shown in Fig. 8A, the covalent pair did demonstrate a better pharmacokinetic profile than the DAR1 ARC.

To investigate the mechanism of pharmacokinetic alteration, we titrated the pair stability in different concentrations of mouse plasma or serum for 2 h at 37°C. We found that both mut4 pair and p19 pair are quite stable in mouse serum, even at 80% (Fig. 8C and Supplementary Fig. S16). However, the mut4 pair can dissociate in mouse plasma of proportion >50%, and p19 pair would not. The proportion-dependent dissociation indicates that siRNA can be displaced by certain components present in plasma but not serum, and the displacement is concentration dependent. This interesting finding led us to screen the abundant components in the coagulation cascade, including some clotting factors, plasma-specific proteins, and biopolymers involved in blood clotting. As shown in Fig. 8D, most clotting factors and plasma proteins

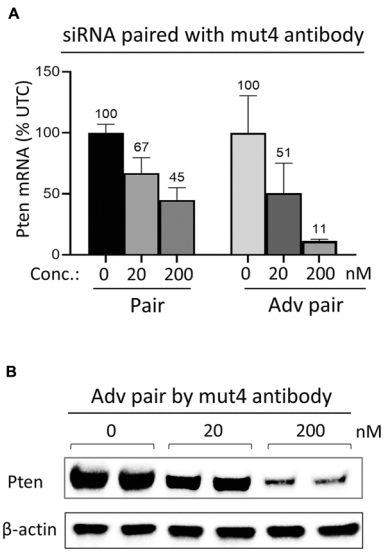

Figure 7. The mut4 antibody was paired with siRNA to knock down Pten mRNA (**A**) and protein (**B**) in NCI-N87 cells after 72-h treatment. UTC, untreated cells.

we tested would not impair the mut4–siRNA binding, but the glycosaminoglycans (GAGs) show a competitive effect to the Stau1 dsRBD domain. The result reveals that Stau1 dsRBD34 is a GAG-binding protein, which has never been reported. We then analyzed the individual role of GAG components, including hyaluronan, chondroitin sulfate, dermatan sulfate, and heparan sulfate (HS) [45]. The ESMA result (right panel in Fig. 8D) shows that HS plays an important role in the siRNA displacement. Chemical structure comparison of GAG disaccharide units reveals that the competition activity has a correlation with the sulfation pattern of GAGs (Fig. 8E). Namely, a higher sulfation density shows stronger displacement ability (fucoidan > HP > HS). It is noted that GAGs, as sulfated glycans, are poorly understood, but their presence/abundance (μM) in plasma has been well reported [46]. With the clarity of displacement mechanism, we are able to design strategies to screen more selective dsRBD mutant on purpose and expand the bifunctional antibody strategy to *in vivo* applications in future.

Discussion

In this study, we harnessed the dsRNA-binding ability of Stau1 dsRBD34 and developed a modular antibody to deliver siRNAs, in a way to circumvent the limitations of current ARC technologies. Stau1 dsRBD34 is chosen over other six dsRBPs owing to its superior siRNA-binding affinity, selectivity, stability, and releasability. Its affinity to siRNA is sequence independent and chemistry tolerable, which enables to bind with all kinds of fully modified siRNAs, including Alt OMe, ESC, adv ESC, and ESC + chemotypes. This feature is important because all therapeutic siRNAs have to be modified extensively to increase the stability and immune safety [47]. Owing to the binding specificity of dsRBD34, the modular antibody achieves a one-to-one pairing with siRNA. The diligent antibody–siRNA pair retains the high-antigen-binding selectivity and demonstrates an effective gene silencing on the antigen-positive cells, albeit influenced by the stoichiometry, time interval of uptake, and siRNA chemotypes.

The Stau1 dsRBD-based modular antibody has an intriguing mechanism of siRNA release in cell cytosols. The dissociation is triggered by displacement of siRNA from dsRBD34 by the cellular RNAs (they have plenty of dsRNA folds in structure). The result is desirable because it means that siRNA can be released from antibody–siRNA pairs and accessible by RNA-induced silencing complex (RISC) once delivered to the cytosol. The siRNA displacement by cellular RNAs is an instant (<1 min) but concentration-dependent step. The competitive test revealed that dsRBD34/siRNA complex could be completely disrupted by 50 ng/μl of cellular RNAs in 1 min. Cellular RNAs are one of the major cellular components which constitute up to 20% of a cell's dry weight. It is present mainly in the crowded cytosol where RNA concentrations can reach 20 μg/μl [48]. Although some RNAs are present as ribonucleoprotein complexes, the extremely rich RNA environment would trigger an instant and complete release of siRNAs from dsRBDs in the cytosol, which facilitates the RISC loading and RNAi response.

We here advanced the antibody–siRNA pairing system by appending siRNA terminus with SM enhancers so as to augment the endosome-to-cytosol import and RNAi potency. We identified two SM enhancers of significant improvement, prazosin and guanabenz, which both are FDA-approved drugs. These two compounds have been reported previously to increase the endosomal escape of protein antigens or hydrophobically modified siRNAs by co-incubating with cells as free forms at high concentrations (>20 μM) [42, 49]. Despite effectiveness, the co-incubation strategy requires a concentration so high that compounds can induce cytotoxicity, which dramatically limits the clinical relevance. A number of mechanisms have been proposed to explain why SM compounds could destabilize endosomal membranes [50–53]. For instance, prazosin and guanabenz as lysomotropic agents, tend to accumulate inside endosomes and induce the lysosomal alkalization, which finally causes the osmotic swelling and leakage [42]. In this study, prazosin is conjugated with siRNA and traffics into endosomes along with the pairs whose concentration is not high (200 nM). Therefore, the trapped prazosin molecules are not so many to trigger the "proton sponge mechanism" as mentioned above. Indeed, we did not observe the presence of enlarged endosome/lysosome vesicles, a phenomenon commonly seen with proton sponge activity [54, 55], in cells treated by the advanced pair. Meanwhile, the most ironic proton-sponge agent—chloroquine—did not show a significant improvement on RNAi potency after siRNA conjugation and pairing with antibody. Combinedly, these results indicated that another mechanism might play a role in the endosome-to-cytosol import. We speculated that the protonated prazosin might prone to insert into the lysosomal membranes, resulting in the fluidization and destabilization of the bilayer. This hypothesis is in agreement with the observation that both free prazosin and its siRNA conjugate can mediate the endosome-to-cytosol import. More studies are required to clarify the mechanism.

A recent report by Wittrup group highlighted that higher affinity against siRNA by siRNA-binding p19 protein could correlate with more potent silencing *in vitro* [25]. However, the antibody–siRNA pairs with a tighter association in this study did not lead to an improved potency. The result is disappointing, but the discrepancy could be explained by the difference in transfection conditions used in two studies. Wittrup group utilized the perfringolysin O (PFO)-based agent

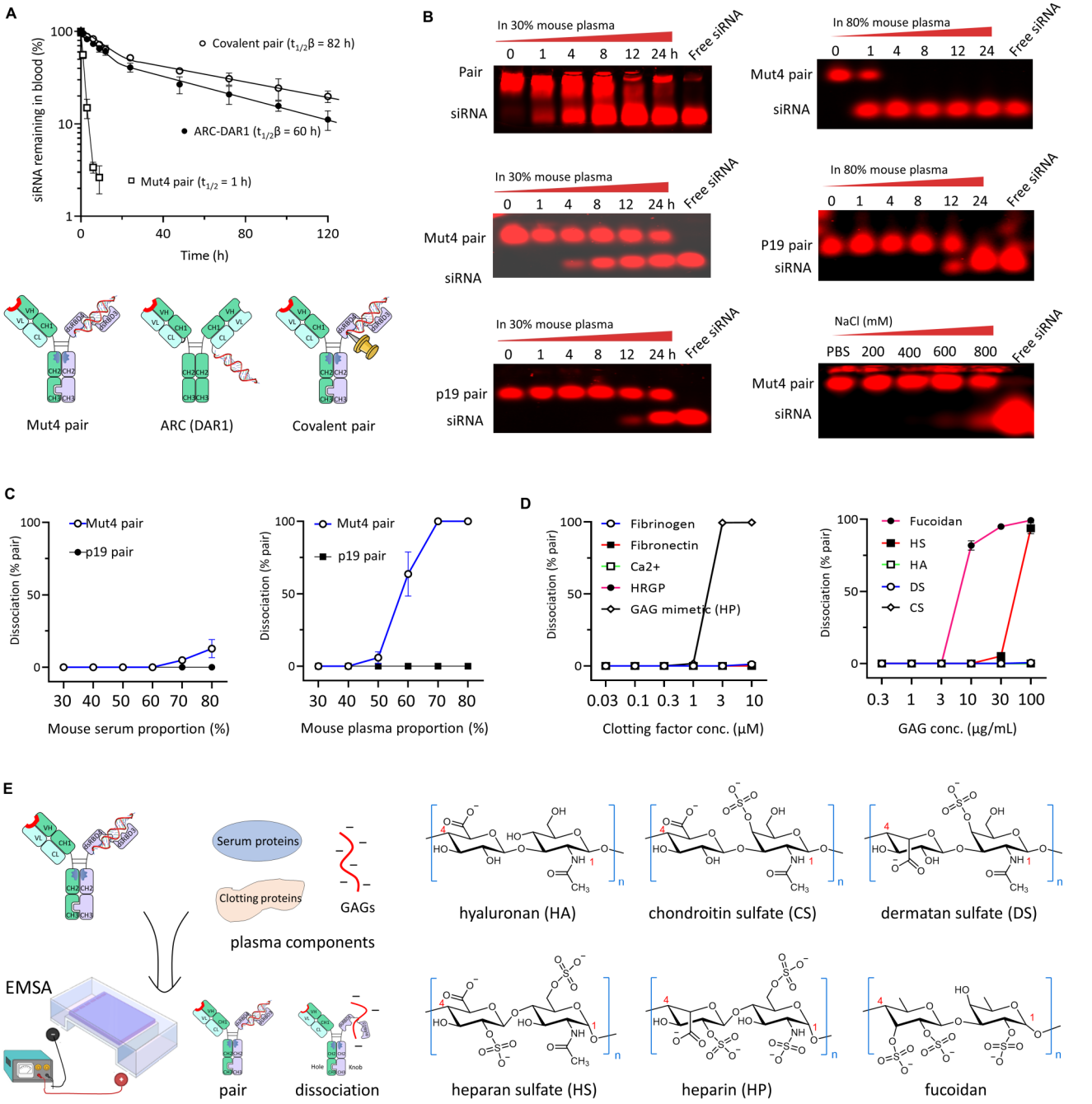

Figure 8. Pharmacokinetics of antibody–siRNA systems and the alteration by competition from plasma components. (**A**) Pharmacokinetics of three systems in BALB/c mice. Covalent pair was obtained by tethering siRNA to a Cys position near the dsRBD domain by thiol–maleimide conjugation $t_{1/2}\beta$, the elimination half-life. (**B**) EMSA assay to test the pair stability in varying conditions at 37°C. SiRNA was labeled by sulfo-Cy7 and loaded at 10 fmol per well. (**C**) Evaluation of pair dissociation tendency in the presence of mouse serum or plasma (2 h, 37°C). (**D**) siRNA displacement from mut4–siRNA pairs by competition of plasma proteins and GAGs (2 h, 37°C). HRGP, histidine-rich glycoprotein. (**E**) Chemical structures of GAGs and the EMSA assay. Fucoidan is a marine GAG and used as a positive control due to its high sulfation density.

to facilitate the delivery of p19/siRNA pairs, which enables to examine the silencing activity of siRNA at the extremely low concentration (0.5 nM), thanks to the super fusogenic activity of PFO [56, 57]. With a purpose of practical significance, we applied a free-uptake approach in this study, albeit its less effectiveness in RNAi. In the high-concentration ranges where the silencing was observed in our study (20–200 nM), the RNAi potency might be independent from the affinity to siRNA. Nevertheless, further study on the affinity maturation might lead to the next-generation antibody–siRNA pairs that can be seen an improvement on RNAi activity.

It is worth noting that dsRBD can mask the negative charges of siRNAs, yielding a nearly charge-neutral antibody–siRNA pair. The charge-balanced feature would mitigate the nonspecific interaction between siRNA payloads and serum proteins, which might maximize the circulation half-lives and *in vivo* performance of pairs *in vivo* [39]. However, the underlying benefit could not be validated in this study due to the instability of antibody–siRNA pair in mouse plasma. By the

diligent protein engineering and evolution, we may enhance the distinguishability of Stau1 dsRBD to siRNA over sulfated GAGs in plasma later. The viral protein p19 and its evolution strategy by Wittrup group could be an example [25]. Altogether, a dsRBD module of ultrahigh affinity and selectivity to siRNA would be essential for the design of bifunctional antibody in the next stage.

In sum, we established an antibody–siRNA pairing platform by utilizing Stau1 dsRBD34 as the key module. The antibody–siRNA pair possesses a diligent one-to-one structure, which resembles the DAR1 ARC, but displays the charge-neutral surface and conjugation-free advantages. We also demonstrated its potential to be further advanced by SM enhancer appendence and dsRBD affinity maturation. Overall, we have created an antibody–siRNA pairing blueprint that we hope will help bring siRNA delivery to the aim of extrahepatic tissues in the future.

Acknowledgement

Author contributions: Yahui Liu (Investigation [equal], Methodology [equal], Writing – original draft [equal]), Yan Zheng (Investigation [equal], Methodology [equal], Validation [equal]), Ruolin Xu (Validation [supporting], Visualization [supporting]), and Yanan Quan (Validation [supporting], Visualization [supporting]).

Supplementary data

Supplementary data is available at NAR online.

Conflict of interest

None declared.

Funding

This work was financially supported by the National Key R&D Program of China (Grant No. 2021YFA0909900) and the National Natural Science Foundation of China (Grant No. 82273860). Funding to pay the Open Access publication charges for this article was provided by the funding grant from National Key R&D Program of China.

Data availability

The data underlying this article will be shared on reasonable request to the corresponding author.

References

1. Cao W, Li R, Pei X *et al.* Antibody–siRNA conjugates (ARC): emerging siRNA drug formulation. *Med Drug Discovery* 2022;15:100128. https://doi.org/10.1016/j.medidd.2022.100128
2. Mullard A. Antibody–oligonucleotide conjugates enter the clinic. *Nat Rev Drug Discov* 2022;21:6–8. https://doi.org/10.1038/d41573-021-00213-5
3. Dowdy SF. Endosomal escape of RNA therapeutics: how do we solve this rate-limiting problem? *RNA* 2023;29:396–401. https://doi.org/10.1261/rna.079507.122
4. Cuellar TL, Barnes D, Nelson C *et al.* Systematic evaluation of antibody-mediated siRNA delivery using an industrial platform of THIOMAB–siRNA conjugates. *Nucleic Acids Res* 2015;43:1189–203. https://doi.org/10.1093/nar/gku1362
5. Malecova B, Burke RS, Cochran M *et al.* Targeted tissue delivery of RNA therapeutics using antibody–oligonucleotide conjugates (AOCs). *Nucleic Acids Res* 2023;51:5901–10. https://doi.org/10.1093/nar/gkad415
6. Cochran M, Arias D, Burke R *et al.* Structure–activity relationship of antibody–oligonucleotide conjugates: evaluating bioconjugation strategies for antibody–siRNA conjugates for drug development. *J Med Chem* 2024;67:14852–67. https://doi.org/10.1021/acs.jmedchem.4c00802
7. Nanna AR, Kel'in AV, Theile C *et al.* Generation and validation of structurally defined antibody–siRNA conjugates. *Nucleic Acids Res* 2020;48:5281–93. https://doi.org/10.1093/nar/gkaa286
8. Matikonda SS, McLaughlin R, Shrestha P *et al.* Structure–activity relationships of antibody–drug conjugates: a systematic review of chemistry on the trastuzumab scaffold. *Bioconjug Chem* 2022;33:1241–53. https://doi.org/10.1021/acs.bioconjchem.2c00177
9. Song E, Zhu P, Lee SK *et al.* Antibody mediated *in vivo* delivery of small interfering RNAs via cell-surface receptors. *Nat Biotechnol* 2005;23:709–17. https://doi.org/10.1038/nbt1101
10. Yao YD, Sun TM, Huang SY *et al.*, Targeted delivery of PLK1–siRNA by ScFv suppresses Her2+ breast cancer growth and metastasis. *Sci Transl Med* 2012;4:130ra48. https://doi.org/10.1126/scitranslmed.3003601
11. Bäumer S, Bäumer N, Appel N *et al.* Antibody-mediated delivery of anti-KRAS-siRNA *in vivo* overcomes therapy resistance in colon cancer. *Clin Cancer Res* 2015;21:1383–94. https://doi.org/10.1158/1078-0432.CCR-13-2017
12. Bäumer N, Appel N, Terheyden L *et al.* Antibody-coupled siRNA as an efficient method for *in vivo* mRNA knockdown. *Nat Protoc* 2016;11:22–36. https://doi.org/10.1038/nprot.2015.137
13. Kumar P, Ban HS, Kim SS *et al.* T cell-specific siRNA delivery suppresses HIV-1 infection in humanized mice. *Cell* 2008;134:577–86. https://doi.org/10.1016/j.cell.2008.06.034
14. Ma Y, Kowolik CM, Swiderski PM *et al.* Humanized Lewis-Y specific antibody based delivery of STAT3 siRNA. *ACS Chem Biol* 2011;6:962–70. https://doi.org/10.1021/cb200176v
15. Ripoll M, Cahuzac H, Dovgan I *et al.* Supramolecular bioconjugation strategy for antibody-targeted delivery of siRNA. *Bioconjug Chem* 2024;35:1503–11.
16. Bäumer N, Scheller A, Wittmann L *et al.* Electrostatic anti-CD33-antibody–protamine nanocarriers as platform for a targeted treatment of acute myeloid leukemia. *J Hematol Oncol* 2022;15:171. https://doi.org/10.1186/s13045-022-01390-5
17. Choi Y-S, Lee JY, Suh JS *et al.* The systemic delivery of siRNAs by a cell penetrating peptide, low molecular weight protamine. *Biomaterials* 2010;31:1429–43. https://doi.org/10.1016/j.biomaterials.2009.11.001
18. Sasso JM, Tenchov R, Bird R *et al.* The evolving landscape of antibody–drug conjugates: in depth analysis of recent research progress. *Bioconjug Chem* 2023;34:1951–2000. https://doi.org/10.1021/acs.bioconjchem.3c00374
19. Gleghorn ML, Maquat LE. 'Black sheep' that don't leave the double-stranded RNA-binding domain fold. *Trends Biochem Sci* 2014;39:328–40. https://doi.org/10.1016/j.tibs.2014.05.003
20. Vuković L, Koh HR, Myong S *et al.* Substrate recognition and specificity of double-stranded RNA binding proteins. *Biochemistry* 2014;53:3457–66.
21. Eguchi A, Meade BR, Chang Y-C *et al.* Efficient siRNA delivery into primary cells by a peptide transduction domain–dsRNA binding domain fusion protein. *Nat Biotechnol* 2009;27:567–71. https://doi.org/10.1038/nbt.1541
22. Geoghegan JC, Gilmore BL, Davidson BL. Gene silencing mediated by siRNA-binding fusion proteins is attenuated by double-stranded RNA-binding domain structure. *Mol Ther - Nucleic Acids* 2012;1:e53. https://doi.org/10.1038/mtna.2012.43
23. Tai W, Li J, Corey E *et al.* A ribonucleoprotein octamer for targeted siRNA delivery. *Nat Biomed Eng* 2018;2:326–37. https://doi.org/10.1038/s41551-018-0214-1

24. Guenther DC, Mori S, Matsuda S *et al.* Role of a "magic" methyl: 2′-deoxy-2′-α-F-2′-β-C-methyl pyrimidine nucleotides modulate RNA interference activity through synergy with 5′-phosphate mimics and mitigation of off-target effects. *J Am Chem Soc* 2022;144:14517–34. https://doi.org/10.1021/jacs.2c01679
25. Yang NJ, Kauke MJ, Sun F *et al.* Cytosolic delivery of siRNA by ultra-high affinity dsRNA binding proteins. *Nucleic Acids Res* 2017;45:7602–14. https://doi.org/10.1093/nar/gkx546
26. Atwell S, Ridgway JB, Wells JA *et al.* Stable heterodimers from remodeling the domain interface of a homodimer using a phage display library. *J Mol Biol* 1997;270:26–35. https://doi.org/10.1006/jmbi.1997.1116
27. Wei H, Cai H, Jin Y *et al.* Structural basis of a novel heterodimeric Fc for bispecific antibody production. *Oncotarget* 2017;8:51037–49. https://doi.org/10.18632/oncotarget.17558
28. Liu Y, Quan Y, Mao Q *et al.* Exploring the potentials of antibody–siRNA conjugates in tumor cell gene silencing without cationic assistance. *Bioconjug Chem* 2025;36:1721–32. https://doi.org/10.1021/acs.bioconjchem.5c00212
29. Chen C, Ridzon DA, Broomer AJ *et al.* Real-time quantification of microRNAs by stem-loop RT-PCR. *Nucleic Acids Res* 2005;33:e179. https://doi.org/10.1093/nar/gni178
30. Chen L, Bosmajian C, Woo S. A highly sensitive stem-loop RT-qPCR method to study siRNA intracellular pharmacokinetics and pharmacodynamics. *Biol Methods Protoc* 2024;9:bpae029. https://doi.org/10.1093/biomethods/bpae029
31. Tian B, Bevilacqua PC, Diegelman-Parente A *et al.* The double-stranded-RNA-binding motif: interference and much more. *Nat Rev Mol Cell Biol* 2004;5:1013–23. https://doi.org/10.1038/nrm1528
32. Doyle M, Jantsch MF. New and old roles of the double-stranded RNA-binding domain. *J Struct Biol* 2002;140:147–53. https://doi.org/10.1016/S1047-8477(02)00544-0
33. Fierro-Monti I, Mathews MB. Proteins binding to duplexed RNA: one motif, multiple functions. *Trends Biochem Sci* 2000;25:241–6. https://doi.org/10.1016/S0968-0004(00)01580-2
34. Yadav DK, Zigáčková D, Zlobina M *et al.* Staufen1 reads out structure and sequence features in ARF1 dsRNA for target recognition. *Nucleic Acids Res* 2020;48:2091–106. https://doi.org/10.1093/nar/gkz1163
35. Almasi S, Jasmin BJ. The multifunctional RNA-binding protein Staufen1: an emerging regulator of oncogenesis through its various roles in key cellular events. *Cell Mol Life Sci* 2021;78:7145–60. https://doi.org/10.1007/s00018-021-03965-w
36. Lazzaretti D, Bandholz-Cajamarca L, Emmerich C *et al.* The crystal structure of Staufen1 in complex with a physiological RNA sheds light on substrate selectivity. *Life Sci Alliance* 2018;1:e201800187. https://doi.org/10.26508/lsa.201800187
37. Bevilacqua PC, Cech TR. Minor-groove recognition of double-stranded RNA by the double-stranded RNA-binding domain from the RNA-activated protein kinase PKR. *Biochemistry* 1996;35:9983–94. https://doi.org/10.1021/bi9607259
38. Zhang M, Huang Y. siRNA modification and delivery for drug development. *Trends Mol Med* 2022;28:892–3. https://doi.org/10.1016/j.molmed.2022.08.003
39. Rocca C, Dennin S, Gu Y *et al.* Evaluation of electrophoretic mobility shift assay as a method to determine plasma protein binding of siRNA. *Bioanalysis* 2019;11:1927–39. https://doi.org/10.4155/bio-2019-0151
40. Lehot V, Kuhn I, Nothisen M *et al.* Non-specific interactions of antibody-oligonucleotide conjugates with living cells. *Sci Rep* 2021;11:5881. https://doi.org/10.1038/s41598-021-85352-w
41. Debacker AJ, Voutila J, Catley M *et al.* Delivery of oligonucleotides to the liver with GalNAc: from research to registered therapeutic drug. *Mol Ther* 2020;28:1759–71. https://doi.org/10.1016/j.ymthe.2020.06.015
42. Kozik P, Gros M, Itzhak DN *et al.* Small molecule enhancers of endosome-to-cytosol import augment anti-tumor immunity. *Cell Rep* 2020;32:107905. https://doi.org/10.1016/j.celrep.2020.107905
43. Prakash TP, Graham MJ, Yu J *et al.* Targeted delivery of antisense oligonucleotides to hepatocytes using triantennary *N*-acetyl galactosamine improves potency 10-fold in mice. *Nucleic Acids Res* 2014;42:8796–807. https://doi.org/10.1093/nar/gku531
44. Masliah G, Barraud P, Allain FH. RNA recognition by double-stranded RNA binding domains: a matter of shape and sequence. *Cell Mol Life Sci* 2013;70:1875–95.
45. Künze G, Huster D, Samsonov SA. Investigation of the structure of regulatory proteins interacting with glycosaminoglycans by combining NMR spectroscopy and molecular modeling—the beginning of a wonderful friendship. *Biol Chem* 2021;402:1337–55.
46. Bratulic S, Limeta A, Maccari F *et al.* Analysis of normal levels of free glycosaminoglycans in urine and plasma in adults. *J Biol Chem* 2022;298:101575. https://doi.org/10.1016/j.jbc.2022.101575
47. Narasipura EA, VanKeulen-Miller R, Ma Y *et al.* Ongoing clinical trials of nonviral siRNA therapeutics. *Bioconjug Chem* 2023;34:1177–97. https://doi.org/10.1021/acs.bioconjchem.3c00205
48. Majumder S, DeMott CM, Reverdatto S *et al.* Total cellular RNA modulates protein activity. *Biochemistry* 2016;55:4568–73. https://doi.org/10.1021/acs.biochem.6b00330
49. Osborn MF, Alterman JF, Nikan M *et al.* Guanabenz (Wytensin™) selectively enhances uptake and efficacy of hydrophobically modified siRNAs. *Nucleic Acids Res* 2015;43:8664–72. https://doi.org/10.1093/nar/gkv942
50. Gillespie EJ, Ho CL, Balaji K *et al.* Selective inhibitor of endosomal trafficking pathways exploited by multiple toxins and viruses. *Proc Natl Acad Sci USA* 2013;110:E4904–12. https://doi.org/10.1073/pnas.1302334110
51. Du Rietz H, Hedlund H, Wilhelmson S *et al.* Imaging small molecule-induced endosomal escape of siRNA. *Nat Commun* 2020;11:1809. https://doi.org/10.1038/s41467-020-15300-1
52. Brock DJ, Kondow-McConaghy HM, Hager EC *et al.* Endosomal escape and cytosolic penetration of macromolecules mediated by synthetic delivery agents. *Bioconjug Chem* 2019;30:293–304. https://doi.org/10.1021/acs.bioconjchem.8b00799
53. Debisschop A, Bogaert B, Muntean C *et al.* Beyond chloroquine: cationic amphiphilic drugs as endosomal escape enhancers for nucleic acid therapeutics. *Curr Opin Chem Biol* 2024;83:102531. https://doi.org/10.1016/j.cbpa.2024.102531
54. Wojnilowicz M, Glab A, Bertucci A *et al.* Super-resolution imaging of proton sponge-triggered rupture of endosomes and cytosolic release of small interfering RNA. *ACS Nano* 2019;13:187–202. https://doi.org/10.1021/acsnano.8b05151
55. Vermeulen LMP, Brans T, Samal SK *et al.* Endosomal size and membrane leakiness influence proton sponge-based rupture of endosomal vesicles. *ACS Nano* 2018;12:2332–45. https://doi.org/10.1021/acsnano.7b07583
56. Yang NJ, Liu DV, Sklaviadis D *et al.* Antibody-mediated neutralization of perfringolysin O for intracellular protein delivery. *Mol Pharm* 2015;12:1992–2000. https://doi.org/10.1021/mp500797n
57. Liu DV, Yang NJ, Wittrup KD. A nonpolycationic fully proteinaceous multiagent system for potent targeted delivery of siRNA. *Mol Ther - Nucleic Acids* 2014;3:e162. https://doi.org/10.1038/mtna.2014.14

Received: July 18, 2025. **Accepted:** December 16, 2025